Research Article Vol. 40, No. 4 / April 2023 / Journal of the Optical Society of America B 705

Journal of the Optical Society of America B

OPTICAL PHYSICS

# Hybrid near-optimum binary receiver with realistic photon-number-resolving detectors

MICHELE N. NOTARNICOLA,[1,2] MATTEO G. A. PARIS,[1,2] AND STEFANO OLIVARES[1,2,*]

[1]Dipartimento di Fisica "Aldo Pontremoli", Università degli Studi di Milano, I-20133 Milano, Italy
[2]Istituto Nazionale di Fisica Nucleare, Sezione di Milano, I-20133 Milano, Italy
*stefano.olivares@fisica.unimi.it

Received 20 July 2022; revised 5 January 2023; accepted 15 January 2023; posted 18 January 2023; published 8 March 2023

**We propose a near-optimum receiver for the discrimination of binary phase-shift-keyed coherent states employing photon-number-resolving detectors. The receiver exploits a discrimination strategy based on both so-called homodyne-like and direct detection, thus resulting in a hybrid scheme. We analyze the performance and robustness of the proposed scheme under realistic conditions, namely, in the presence of inefficient detection and dark counts. We show that the present hybrid setup is near- optimum and beats both the standard quantum limit and the performance of the Kennedy receiver.** 

https://doi.org/10.1364/JOSAB.470806

## 1. INTRODUCTION

The problem of discriminating quantum states is a challenging task in quantum information theory, since quantum mechanics does not allow perfect discrimination if the considered states are not orthogonal. In particular, the task of coherent state discrimination is of great relevance for quantum communications, since these states are the typical information carrier in optical channels, finding a large application in both physics and telecommunication engineering [1]. The simplest scenario is binary phase shift keying (BPSK), where one has to discriminate between two coherent states with the same energy but a $\pi$ phase difference [1–3]. In this case, the theory developed by Helstrom [2,3] identifies the minimum error probability, the so-called Helstrom bound, raising the question concerning the possible implementation of an optimal receiver able to achieve this bound.

Several proposals of feasible optimum or near-optimum receivers have been advanced in literature, based on either single-shot discrimination or feedback-based strategies. As regards single-shot strategies, there are several options. Homodyne receivers [1] are constructed as an extension of the classical systems for discrimination of signals and are based on the measurement of the quadratures of the optical field. The Kennedy receiver [4] is based on a nulling displacement operation followed by photodetection and proves to be near-optimum, reaching in the high energy regime twice the Helstrom bound. Recently, such a scheme has also been improved by Takeoka and Sasaki [5] by optimizing the displacement operation, obtaining a further advantage in the range of small energies. Finally, Sasaki and Hirota [6] have proposed a scheme that is able to reach the Helstrom bound based on the application of unitary operations defined in the two-dimensional space spanned by coherent states. However, the realization of such unity would require highly non-linear optical elements, making this kind of receiver not realizable with the usual practical linear optics components.

Better results are obtained with feedback strategies. Dolinar [7] extended the principle of the Kennedy receiver by designing a new receiver employing a time-varying displacement operation conditioned on the outcome of continuous photodetection. The Dolinar receiver is indeed optimum and reaches the Helstrom bound. More recently, the Dolinar approach has been revised, and less demanding strategies have been proposed that employ feed-forward methods exploiting the *slicing* of the coherent state. In these discrimination strategies, the incoming state is split into a finite number of copies with smaller energies, and each copy is measured conditioning a unitary operation on the following one [8–10].

In this paper. we address single-shot binary discrimination in realistic conditions. In particular, we propose a hybrid scheme based on the combination of homodyne-like and direct detection and prove it to be robust against detector inefficiencies and phase noise affecting the input signals. In more detail, we exploit a homodyne setup that we call *homodyne-like*, where the usual p-i-n photodiodes are replaced with photon-number-resolving (PNR) detectors having a finite photon number resolution [11], and a low local oscillator (LO) is considered [12,13]. Good candidates as PNR detectors are hybrid photodetectors, which are endowed with partial photon number resolution and a linear response up to 100 photons [14], though with a quantum efficiency of about 50% in the green spectral region. Very high quantum efficiencies are obtained with transition-edge sensors (TESs), but their dynamic range falls to approximatively 10 photons. Interestingly, these detectors have been recently

used to implement homodyne-like detection schemes [15,16]. Therefore, in our theoretical analysis, we include the presence of quantum efficiency $\eta < 1$, and also of a non-zero dark count rate $\nu$ and visibility reduction $\xi < 1$.

The structure of the paper is the following. In Sections 2 and 3, we recall the basics of binary discrimination theory and describe the features of homodyne-like detection, respectively. Then, in Section 4, we present our proposal of a hybrid receiver employing both homodyne-like and direct detection schemes and considering ideal PNRs. In Section 5, we show the robustness of the hybrid receiver against detection inefficiencies (such as finite resolution of PNRs, quantum efficiency, dark counts, and interference visibility). Section 6 closes the paper with some concluding remarks.

## 2. BINARY DISCRIMINATION OF COHERENT SIGNALS

The theory of quantum discrimination between non-orthogonal states has been addressed by Helstrom [2]. In a general framework, a sender encodes a classical symbol "0" or "1" onto two quantum states $|\psi_0\rangle$ and $|\psi_1\rangle$ with *a priori* probabilities $q_0$ and $q_1$, respectively. The states are sent through a communication channel and a receiver performs a positive-operator-valued measure (POVM) to infer the encoded values 0 or 1. If $p(j|k)$ $(j, k \in \{0, 1\})$ is the conditional probability of obtaining the outcome $j$ if $k$ was sent, then the receiver discriminates the states with an error probability $P_{\rm err} = q_0 p(1|0) + q_1 p(0|1)$. The task is to find an optimal POVM that minimizes $P_{\rm err}$, and the corresponding receiver is referred to as *optimum*.

Here we address the discrimination of two pure *coherent states* of a single-mode optical field, that is, states of the form $|\zeta\rangle = D(\zeta)|0\rangle$, $\zeta \in \mathbb{C}$, where $D(\zeta) = \exp(\zeta a^\dagger - \zeta^* a)$ is the displacement operator, $a$ is the field operator, $[a, a^\dagger] = 1$, and $|0\rangle$ is the vacuum state. In particular, we consider a BPSK scheme, where the two states to be discriminated are

$$|\alpha_0\rangle = |-\alpha\rangle \quad \text{and} \quad |\alpha_1\rangle = |\alpha\rangle, \tag{1}$$

having the same energy $|\alpha|^2$ but opposite phases (a $\pi$ phase shift). In the following, we focus on the case of equal *a priori* probabilities $q_0 = q_1 = 1/2$, and, without loss of generality, we assume $\alpha \in \mathbb{R}_+$.

Helstrom's theory allows to compute the minimum error probability, the corresponding *Helstrom bound*, which reads

$$P_{\rm Hel} = \frac{1}{2}\left[1 - \sqrt{1 - 4q_0 q_1 |\langle\alpha_0|\alpha_1\rangle|^2}\right] \tag{2}$$

$$= \frac{1}{2}\left[1 - \sqrt{1 - e^{-4\alpha^2}}\right]. \tag{3}$$

The optimal measurement strategy achieving such a minimum is the *"cat state" measurement*, defined by the two-valued POVM $\{\Pi_0, \mathbb{1} - \Pi_0\}$, $\Pi_0 = |\psi_{\rm cat}\rangle\langle\psi_{\rm cat}|$, where $|\psi_{\rm cat}\rangle = c_0(\alpha)|\alpha_0\rangle + c_1(\alpha)|\alpha_1\rangle$ is an optimized cat state [2]. However, a concrete realization of such a POVM is not an easy task, and therefore, there exist many alternative feasible schemes. Here we introduce the *Kennedy receiver*, which will be taken as a benchmark throughout the whole paper.

The Kennedy receiver [4], also known as a *displacement receiver*, consists of the application of a fixed displacement operation $D(\alpha)$ applied to each of the two pulses sent, with the effect of mapping

$$|-\alpha\rangle \to |0\rangle \quad \text{and} \quad |\alpha\rangle \to |2\alpha\rangle. \tag{4}$$

This can be seen as a *nulling operation* able to send to the vacuum one of the two input signals. The displacement can be implemented by mixing the incoming signals with a properly chosen LO at a beam splitter with suitable transmissivity. Then, the discrimination problem is turned into vacuum discrimination, which can be performed by employing an on–off detector, leading to the error probability

$$P_K = \frac{|\langle 0|2\alpha\rangle|^2}{2} = \frac{e^{-4\alpha^2}}{2}. \tag{5}$$

Although $P_K > P_{\rm Hel}$, such receiver is *near-optimum*, since in the regime $\alpha^2 \gg 1$, we have $P_K \approx 2P_{\rm Hel}$.

In the following, we will consider a generalization of the Kennedy receiver, which we will refer to as a *displacement-PNR*(D-PNR) receiver, where the on–off detector is replaced by a PNR detector. As will be discussed throughout the paper, the photon number resolution of the detector will turn out to be useful to improve the decision strategy in the presence of realistic inefficiencies of the receiver.

## 3. HOMODYNE-LIKE MEASUREMENT

With homodyne-like detection, we refer to a homodyne setup that involves PNR detectors rather than common photodiodes [12]. In this scheme, the input state described by the density operator $\rho$ interferes at a balanced beam splitter with a low-intensity LO, prepared in the coherent state $|z\rangle$, $z \in \mathbb{R}_+$. Then, PNR detection is performed on the beams outgoing the beam splitter, having access to the statistics of photon numbers $n$ and $m$. Finally, we compute the difference photocurrent $\Delta = n - m$, $\Delta \in \mathbb{Z}$ (see Fig. 1).

In the case of our interest, we consider a coherent input state $\rho = |\zeta\rangle\langle\zeta|$, $\zeta \in \mathbb{C}$. Then, the photocurrent $\Delta$ is the difference

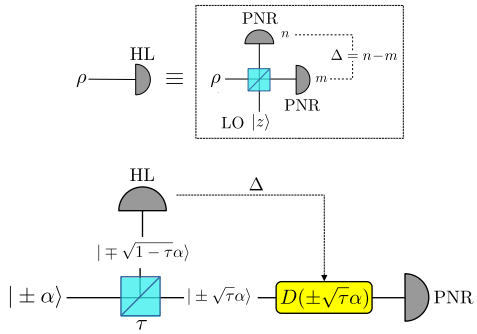


**Fig. 1.** (Top) Implementation of homodyne-like detection. The incoming signal is mixed at a balanced beam splitter with a low local oscillator (LO), and then PNR detection is performed on the two branches. (Bottom) Scheme of the hybrid receiver discussed in the paper. The input coherent state is split at a beam splitter of variable transmissivity $\tau$. On the reflected beam, we perform homodyne-like detection, whose outcome $\Delta$ conditions a displacement operation on the transmitted signal. After that, we apply on–off measurement on it.

of two Poisson random variables and therefore follows a *Skellam distribution* [12]:

$$S(\Delta;\zeta)=e^{-\mu_c(\zeta)-\mu_d(\zeta)}\left[\frac{\mu_c(\zeta)}{\mu_d(\zeta)}\right]^{\Delta/2} I_\Delta(2\sqrt{\mu_c(\zeta)\mu_d(\zeta)}), \tag{6}$$

$\Delta\in\mathbb{Z}$, where

$$\mu_c(\zeta)=\frac{|\zeta+z|^2}{2}, \quad \text{and} \quad \mu_d(\zeta)=\frac{|\zeta-z|^2}{2}, \tag{7}$$

and $I_\Delta(x)$ is the modified Bessel function of the first kind. It is worth noting that in the regime $z^2\gg|\zeta|^2$,

$$S(\Delta;\zeta)\to\frac{\mathcal{P}(x=\Delta/(\sqrt{2}z);\zeta)}{\sqrt{2}z}, \tag{8}$$

where

$$\mathcal{P}(x;\zeta)=\frac{1}{\sqrt{\pi}}\exp\left[-\left(x-\sqrt{2}\zeta\right)^2\right] \tag{9}$$

is the homodyne probability distribution [17].

The scheme described above can be used to implement a *homodyne-like receiver* [13], based on the measured outcome of the photon number difference: if $\Delta<0$, we decide 0; if $\Delta>0$, we decide 1; and if $\Delta=0$, we perform a random choice. The resulting error probability reads

$$P_{HL}=\frac{1}{2}\left[\sum_{\Delta<0}S(\Delta;\alpha)+\sum_{\Delta>0}S(\Delta;-\alpha)\right]+\frac{S_0}{2}, \tag{10}$$

with $S_0=S(0;\alpha)=S(0;-\alpha)$. According to Eq. (8), in the limit $z^2\gg|\zeta|^2$, we regain the traditional *homodyne receiver* whose corresponding error probability reads

$$\begin{aligned}P_H&=\frac{1}{2}\left[\int_0^\infty \mathrm{d}x\mathcal{P}(x;\alpha_0)+\int_{-\infty}^0 \mathrm{d}x\mathcal{P}(x;\alpha_1)\right]\\&=\frac{1-\mathrm{erf}\left(\sqrt{2}\alpha\right)}{2},\end{aligned} \tag{11}$$

known as standard quantum limit (SQL), where $\mathrm{erf}(x)$ is the error function.

In the next section, we will see how we can exploit both the direct detection and homodyne-like receiver to reduce the discrimination error probability. Since the receiver uses at the same time the two detection strategies, we refer to it as *hybrid receiver*.

## 4. NEAR-OPTIMUM HYBRID RECEIVER

The scheme of the hybrid receiver proposed in this paper is depicted in Fig. 1. The idea is to exploit a D-PNR setup where the nulling displacement is not assigned *a priori*, but is conditioned on the outcome of homodyne-like detection performed on a fraction of the input signal. In more detail, we split the input coherent state $|\alpha_{0/1}\rangle=|\mp\alpha\rangle$ at a beam splitter of variable transmissivity $\tau$ (this can be obtained, for instance, considering the polarization of input states and by using a polarizing beam splitter), such that

$$|\mp\alpha\rangle\otimes|0\rangle\to|\mp\sqrt{\tau}\alpha\rangle\otimes|\pm\sqrt{1-\tau}\alpha\rangle. \tag{12}$$

**Table 1. Decision Strategy for the Hybrid Receiver Depicted in Fig. 1**

| Outcomes | Decision |
|---|---|
| $\Delta\geq0$ off | 0 |
| $\Delta<0$ on | 0 |
| $\Delta<0$ off | 1 |
| $\Delta\geq0$ on | 1 |

Then, we perform homodyne-like detection on the reflected branch:

$$|\alpha_{0/1}^{(r)}\rangle=|\pm\sqrt{1-\tau}\alpha\rangle. \tag{13}$$

After that, we apply a feed-forward nulling displacement operation on the transmitted part of the signal conditioned on the outcome $\Delta$ of the homodyne-like measurement:

$$\Delta\geq0\to\text{apply } D\left(\sqrt{\tau}\alpha\right), \tag{14a}$$

$$\Delta<0\to\text{apply } D\left(-\sqrt{\tau}\alpha\right). \tag{14b}$$

Finally, on the resulting displaced state, we perform a PNR measurement in terms of on–off detection: the photon number resolution of the detector will turn out to be useful in the presence of dark counts and visibility reduction, as we will see in the following. The intuitive motivation behind the feed-forward rule of Eq. (14) is the following. If we suppose that $|\alpha_0\rangle$ was sent, from the definition of the beam splitter operation of Eq. (12), it is more likely to obtain $\Delta>0$. As a consequence, we decide to perform a positive displacement sending the transmitted signal into the vacuum such that the PNR detector does not click, and we refer to this event as "off." Of course, there is still a non-zero probability to get $\Delta<0$, and in that case, we decide to apply a negative displacement such that the on–off detector is more likely to count some photon. This event is called "on." Finally, for the case of $\Delta=0$, the displacement amplitude is chosen to be positive simply by convention. Analogous considerations may be obtained by considering state $|\alpha_1\rangle$. Given this scenario, the *decision rule* at the end of the final measurement is chosen according to Table 1.

Since

$$p(\Delta\geq0;\text{on}|0)=p(\Delta<0;\text{off}|1)=0, \tag{15}$$

the error probability for the hybrid receiver is equal to

$$\begin{aligned}P_{\text{hyb}}(\tau)&=\frac{1}{2}\left[\,p(\Delta<0;\text{off}|0)+p(\Delta\geq0;\text{off}|1)\right]\\&=\frac{1}{2}\left[\sum_{\Delta<0}S(\Delta;\alpha_0^{(r)})e^{-4\tau\alpha^2}+\sum_{\Delta\geq0}S(\Delta;\alpha_1^{(r)})e^{-4\tau\alpha^2}\right]\\&=\frac{e^{-4\tau\alpha^2}}{2}\left[\sum_{\Delta<0}S(\Delta;\sqrt{1-\tau}\alpha)+\sum_{\Delta\geq0}S(\Delta;-\sqrt{1-\tau}\alpha)\right],\end{aligned} \tag{16}$$

where we used the Skellam distribution in Eq. (6). For completeness, we note that performing standard homodyne detection instead of homodyne-like, the error probability of the previous equation becomes

$$P_{\rm hyb}^{(\rm HD)}(\tau)=\frac{e^{-4\tau\alpha^2}}{2}\left\{1-\mathrm{erf}\left[\sqrt{2(1-\tau)}\alpha\right]\right\}. \tag{17}$$

Note that if $\tau=0$, we have the homodyne receiver, whereas if $\tau=1$, we retrieve the Kennedy one. This can be understood since when $\tau=1$, the information coming from the homodyne receiver is inconclusive, as it measures the vacuum leading to a positive or negative outcome with 50% probability. Therefore, knowing the outcome sign, we can apply the same inference strategy as in the Kennedy receiver.

Equation (16) depends on $\tau$, and therefore, we can optimize it by finding the transmissivity $\tau_{\rm opt}$, which in general is a function of $\alpha^2$, minimizing the value of $P_{\rm hyb}(\tau)$ for every $\alpha^2$. Consequently, we obtain the optimized error probability of our receiver $P_{\rm hyb}(\tau_{\rm opt})$. To better enlighten the advantages of the hybrid receiver, it is also relevant to introduce the ratio with the standard Kennedy receiver in Eq. (5):

$$R_{h/K}=\frac{P_{\rm hyb}(\tau_{\rm opt})}{P_K}. \tag{18}$$

Plots of $R_{h/K}$ and $\tau_{\rm opt}$ (in the inset) are displayed in the top panel of Fig. 2. It emerges that $\tau_{\rm opt}=0$ up to a threshold energy $N_{\rm th}(z)$, which depends on the LO amplitude $z$, while for $\alpha^2>N_{\rm th}(z)$, it is an increasing function of the energy and reaches asymptotically 1. Note that in the limit $\tau\to 1$, some information about the signal reaches the homodyne receiver, and we still have an improvement in performance. If $\alpha^2\le N_{\rm th}(z)$, the optimized strategy is realized with the sole homodyne-like setup, whereas for larger energies, the more efficient scheme is obtained by the appropriate interplay between the homodyne-like and D-PNR parts of our receiver. The

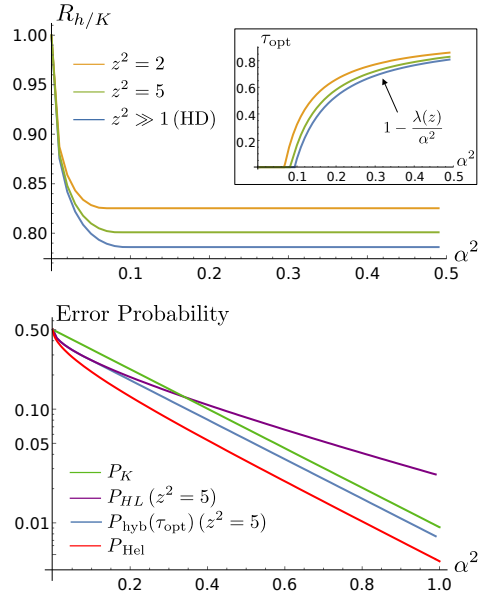


**Fig. 2.** (Top) Plot of the ratio $R_{h/K}$ as a function of the energy $\alpha^2$ of encoded pulses for several values of LO intensity $z^2$. In the inset, plot of the optimized transmissivity $\tau_{\rm opt}$ as a function of $\alpha^2$. For $\alpha^2>N_{\rm th}(z)$, we have $\tau_{\rm opt}=1-\lambda(z)/\alpha^2$. (Bottom) Logarithmic plot of the error probabilities as a function of $\alpha^2$ of the proposed hybrid scheme $P_{\rm hyb}(\tau_{\rm opt})$ compared to the Kennedy receiver [Eq. (5)], homodyne-like receiver [Eq. (10)], and Helstrom bound [Eq. (2)]. Here we fix the LO intensity for the homodyne-like receiver and hybrid receiver to the value $z^2=5$.

choice of the optimal $\tau$ makes the receiver *near-optimum* (see the bottom panel of Fig. 2) with a ratio $R_{h/K}$ saturating to the value $R_\infty<1$ for every value of the LO intensity.

As we noticed, if we increase the intensity of the LO $|z\rangle$, the performance of homodyne-like detection approaches the standard homodyne one. In fact, the variance of the homodyne-like quadrature probability distribution decreases as the LO energy becomes quite larger with respect to the input signal one [18]. In this case, the ratio in Eq. (18) reads

$$R_{h/K}^{(\rm HD)}=\frac{P_{\rm hyb}^{(\rm HD)}}{P_K}=\frac{e^{4(1-\tau)\alpha^2}}{2}\left\{1-\mathrm{erf}\left[\sqrt{2(1-\tau)}\alpha\right]\right\}. \tag{19}$$

The saturation of $R_{h/K}$ for large $\alpha^2$ suggests the following *ansatz* on the expression of the optimized $\tau_{\rm opt}$, namely,

$$\tau_{\rm opt}=1-\frac{\lambda(z)}{\alpha^2}\quad\text{for}\quad\alpha^2>N_{\rm th}(z), \tag{20}$$

where $\lambda(z)\in\mathbb{R}_+$ and depends on the LO amplitude $z$. As an example, for the homodyne limit $z^2\to\infty$, by computing the derivative of Eq. (19) with respect to $\tau$ and inserting the expression in Eq. (20), we get the following relation that must be satisfied by $\lambda\equiv\lambda(z=\infty)$:

$$\sqrt{\frac{2}{\pi\lambda}}-4e^{2\lambda}\left[1-\mathrm{erf}(\sqrt{2\lambda})\right]=0, \tag{21}$$

which leads to the numerical solution $\lambda\approx 0.094$. Then, the threshold $N_{\rm th}^{(\rm HD)}\equiv N_{\rm th}(z=\infty)$ can be obtained by setting $\tau_{\rm opt}=0$, bringing us to $N_{\rm th}^{(\rm HD)}=\lambda$, and the saturation ratio reads

$$R_\infty^{(\rm HD)}=e^{4\lambda}[1-\mathrm{erf}(\sqrt{2\lambda})]\approx 0.786\,. \tag{22}$$

An identical analysis can be performed for the homodyne-like case, where we may expect $\lambda(z)<\lambda$.

## 5. ROBUSTNESS AGAINST DETECTOR INEFFICIENCIES

To investigate the robustness of our scheme, we now consider a more realistic scheme of the hybrid receiver where we assume to have PNR detectors with non-unit quantum efficiency, dark counts, and finite resolution, namely, the detector can resolve up to a given number of photons. Moreover, since the displacement operation is achieved by means of the interference at a beam splitter between the signal and a suitable coherent state, as mentioned above, we also address how non-unit visibility affects the performance of the receiver.

### A. Finite Resolution of PNR Detectors

Realistic PNR detectors have a finite photon number resolution, that is, they can resolve any number of photons $n$ up to $M$; to highlight this feature, we write PNR($M$). For instance, PNR(3) refers to a detector that has only four possible outcomes, $n\in\{0,\,1,\,2,\,\ge 3\}$, where "$\ge 3$" means three or more photons. Clearly, PNR(1) is an on–off photodetector.

PNR($M$) detection may be described through the finite-valued POVM $\{\Pi_n\}_n$, $n=0,\ldots,M$, where

$$\Pi_n = |n\rangle\langle n| \quad \text{for} \quad n = 0, \ldots, M-1, \tag{23}$$

$$\Pi_M = \mathbb{1} - \sum_{n=0}^{M-1} \Pi_n. \tag{24}$$

As a consequence, if we are performing a PNR($M$) measurement on a generic coherent state $|\zeta\rangle$ ($\zeta \in \mathbb{C}$), the probability of detecting the outcome $n$ reads

$$p^{(M)}(n;\, N) = \langle\zeta|\Pi_n|\zeta\rangle = \begin{cases} e^{-N}\dfrac{N^n}{n!} & n < M, \\ 1 - e^{-N}\displaystyle\sum_{j=0}^{M-1}\dfrac{N^j}{j!} & n = M, \end{cases} \tag{25}$$

with a mean photon number $N = |\zeta|^2$.

For the receiver proposed in this paper, the exploitation of a PNR($M$) affects the homodyne-like detector. In fact, given Eq. (25), the probability of getting the photon number difference $\Delta$ after the measurement on the reflected signal 13 reads

$$\mathcal{S}(\Delta;\, \alpha_{0/1}^{(r)}) = \sum_{n=0}^{M}\sum_{m=0}^{M} \delta_{n-m,\Delta}\, p^{(M)}\left(n;\, \mu_c\left(\alpha_{0/1}^{(r)}\right)\right) p^{(M)}\left(m;\, \mu_d\left(\alpha_{0/1}^{(r)}\right)\right), \tag{26}$$

where $\Delta = -M, \ldots, M$, with $\mu_{c/d}$ given in Eq. (7), and $\delta_{k,j}$ is the Kronecker delta. In the limit $M \gg 1$, $\mathcal{S}(\Delta;\, \alpha_{0/1}^{(r)})$ approaches the Skellam distribution in Eq. (6).

The error probability for the hybrid receiver in the presence of PNR($M$) is then equal to

$$P_{\text{hyb}}^{(M)}(\tau) = \frac{e^{-4\tau\alpha^2}}{2}\left[\sum_{\Delta=-M}^{-1}\mathcal{S}(\Delta;\, \alpha_0^{(r)}) + \sum_{\Delta=0}^{M}\mathcal{S}(\Delta;\, \alpha_1^{(r)})\right], \tag{27}$$

which can be optimized to find the transmissivity $\tau_{\text{opt}}(M)$, which shows a behavior qualitatively equivalent to that depicted in Fig. 2. The ratio

$$R_{h/K}(M) = \frac{P_{\text{hyb}}^{(M)}(\tau_{\text{opt}}(M))}{P_K} \tag{28}$$

is depicted in Fig. 3. The effect of the finite resolution is to decrease the saturation ratio $R_\infty(M)$, which in any case is still less than one, maintaining the advantages of our receiver with respect to the Kennedy.

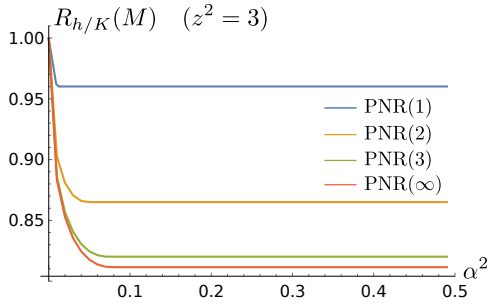


**Fig. 3.** Plot of the ratio $R_{h/K}(M)$ as a function of $\alpha^2$ for several values of the PNR resolution $M$. With the notation PNR($\infty$), we refer to the case of ideal PNR. We fix a LO intensity to be equal to $z^2 = 3$.

### B. Quantum Efficiency $\eta$

Concerning the inefficient photodetection, the introduction of quantum efficiency $\eta$ has the effect of re-scaling all the coherent amplitudes of the measured pulses by a factor $\sqrt{\eta}$, since it corresponds to a photon loss.

For the *Kennedy receiver* employing inefficient on–off detection, the error probability is changed into

$$P_K(\eta) = \frac{e^{-4\eta\alpha^2}}{2}. \tag{29}$$

Instead, for the *hybrid receiver*, the efficiency affects both homodyne-like and PNR measurement schemes. For homodyne-like detection, we have $\mu_c \to \eta\mu_c$ and $\mu_d \to \eta\mu_d$, respectively, obtaining

$$\mathcal{S}_\eta\left(\Delta;\, \alpha_{0/1}^{(r)}\right) = \sum_{m=0}^{M}\delta_{n-m,\Delta}\, p^{(M)}\left(n;\, \eta\mu_c\left(\alpha_{0/1}^{(r)}\right)\right) p^{(M)}\left(m;\, \eta\mu_d\left(\alpha_{0/1}^{(r)}\right)\right). \tag{30}$$

On the other hand, an inefficient on–off detection by the PNR implies the substitution $\exp(-4\tau\alpha^2) \to \exp(-4\eta\tau\alpha^2)$. By performing these substitutions in Eq. (27), we get the corresponding error probability

$$P_{\text{hyb}}^{(M)}(\tau;\, \eta) = \frac{e^{-4\eta\tau\alpha^2}}{2}\left[\sum_{\Delta=-M}^{-1}\mathcal{S}_\eta(\Delta;\, \alpha_0^{(r)}) + \sum_{\Delta=0}^{M}\mathcal{S}_\eta(\Delta;\, \alpha_1^{(r)})\right], \tag{31}$$

and the optimization procedure leads to a different optimized transmissivity $\tau_{\text{opt}}(M, \eta)$, which shows the same qualitative behavior depicted in Fig. 2. The optimized $P_{\text{hyb}}^{(M)}(\tau_{\text{opt}}(M, \eta); \eta)$ is depicted in the top panel of Fig. 4. For a given value of $\eta$, exploiting the hybrid receiver is still preferable to the Kennedy, and the ratio

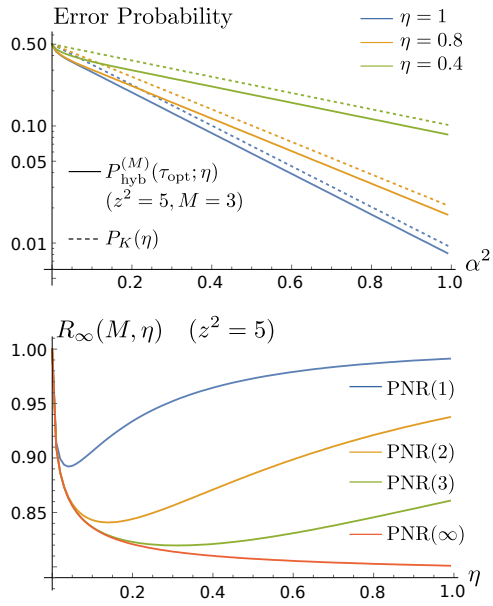


**Fig. 4.** (Top) Logarithmic plot of the error probability of the hybrid receiver employing PNR($M$) detectors and the Kennedy receiver as a function of $\alpha^2$ for several values of $\eta$. Here $M = 3$. (Bottom) Plot of the saturation ratio $R_\infty(M;\, \eta)$ as a function of quantum efficiency $\eta$ for several PNR($M$). The LO intensity for both plots is $z^2 = 5$.

$$R_{h/K}(M,\eta)=\frac{P_{\rm hyb}^{(M)}(\tau_{\rm opt}(M,\eta);\eta)}{P_K(\eta)} \tag{32}$$

still saturates to a value $R_\infty(M,\eta)$, which depends on $\eta$. The plot of the saturation $R_\infty(M,\eta)$ as a function of $\eta$ is depicted in the bottom plot of Fig. 4. If $M=\infty$, the saturation ratio is monotonic and the minimum is achieved for $\eta=1$. On the contrary, since the value of $\eta$ re-scales the counting rates and reduces the negative consequences induced by the truncation of the Poisson distribution up to $M$, with a resolution $M<\infty$, the function is no longer monotonic. Therefore, if $\eta$ is larger than a given threshold value, the ratio $R_\infty(M,\eta)$ increases with efficiency, whereas for smaller $\eta$, the efficiency is too low, and $R_\infty(M,\eta)$ behaves as a decreasing function. Note that for $M<\infty$, the curves exhibit a minimum at a given $\eta$, whose actual value approaches one as $M\to\infty$.

### C. Dark Count Rate $\nu$

Dark counts are random clicks of the PNR due to environmental noise and so not directly correlated to the properties of the coherent measured pulse. Dark counts can be described in terms of Poisson counting [19], occurring at rate $\nu$, which in many realistic conditions takes values $\nu\lesssim 10^{-3}$ [20–24]. Generally speaking, the outcome $n$ of an ideal PNR measurement on a generic coherent state $|\zeta\rangle$ in the presence of dark counts turns out to be the sum of two Poisson variables and therefore still follows a Poisson distribution with a rate equal to $|\zeta|^2+\nu$. [The sum of two Poisson independent random variables is still a Poisson random variable. If $x\sim\mathbb{P}(\mu)$ and $y\sim\mathbb{P}(\lambda)$ are two Poisson independent random variables with rates $\mu$ and $\lambda$, respectively, the probability that $x+y$ gets the value $k$ reads $p(x+y=k)=\sum_{l=0}^{k}p(x=l)p(y=k-l)=e^{-\mu-\lambda}\sum_{l=0}^{k}\mu^l\lambda^{k-l}/(l!(k-l)!)=e^{-\mu-\lambda}(\mu+\lambda)^k/k!\sim\mathbb{P}(\mu+\lambda)$]. In the presence of a PNR($M$), we have a probability $p^{(M)}(n;N)$ as in Eq. (25) but with the rate $N=|\zeta|^2+\nu$.

The presence of dark counts has a significant effect on the performances of quantum receivers. In particular, we will now consider as a benchmark the D-PNR($M$) receiver (D-PNRM) rather than the Kennedy receiver, and exploit the photon number resolution to choose the decision rule for discrimination in a more accurate way. Clearly, the D-PNRM receiver with $M=1$ performs as the Kennedy. Thus, the analysis will proceed in two steps, discussing first the cases of D-PNRM and then approaching the hybrid receiver proposed. Without loss of generality, in the following, we will assume $\eta=1$.

**D-PNRM receiver.** In the presence of dark counts, employing a PNR($M$) detector after the displacement operation rather than an on–off detector brings some advantages. Indeed, in such a situation, the PNR may click even if the vacuum is measured, vanishing the principle behind the nulling technique. As a consequence, the decision rule should be changed according to the maximum *a posteriori* probability (MAP) criterion, discussed in Appendix A. If $|\alpha_0\rangle$ is sent, the probability of detecting $n$ photons is $p^{(M)}(n;\nu)$, whereas if $|\alpha_1\rangle$ is sent, the probability is $p^{(M)}(n;4\alpha^2+\nu)$. The error probability for the D-PNRM receiver is then obtained as

$$P_D(M,\nu)=1-\frac{1}{2}\sum_{n=0}^{M}\max[p^{(M)}(n;\nu),\,p^{(M)}(n;4\alpha^2+\nu)]. \tag{33}$$

The procedure of maximizing the *a posteriori* probability is equivalent to defining a discrimination threshold $n_{\rm th}(\nu)$ such that all measurement outcomes $n\geq n_{\rm th}(\nu)$ are assigned to state 1, and all $n<n_{\rm th}(\nu)$ are assigned to state 0. The threshold number is obtained requiring $p^{(M)}(n_{\rm th};\nu)=p^{(M)}(n_{\rm th};4\alpha^2+\nu)$ and reads

$$n_{\rm th}(\nu)=\min\left[\left\lceil\frac{4\alpha^2}{\ln\left(1+4\alpha^2/\nu\right)}\right\rceil,M\right], \tag{34}$$

where $\lceil\cdot\rceil$ is the ceiling function. We note that the threshold is a function of $\alpha^2$. For the case of PNR(1), we have $n_{\rm th}(\nu)=1$, retrieving the on–off discrimination of the standard Kennedy receiver.

Plots of the error probabilities for different PNR($M$) are depicted in Fig. 5, where it emerges that dark counts have a drastic effect on large energies, making the error probability saturating. The origin of such an effect may be addressed to the finite resolution $M$ of the PNR. Indeed, if $\alpha^2$ is large enough, according to Eq. (34), the discrimination threshold will be chosen as $n_{\rm th}(\nu)=M$; thus, the sole outcome $M$ will infer state 1, and all other outcomes smaller than $M$ will infer state 0. In such a situation, the receiver makes the wrong decision only if an $M$ outcome were actually induced by the state $|\alpha_0\rangle$. Then, the error probability for large $\alpha^2$ should be

$$P_D(M,\nu)\approx\frac{p^{(M)}(M;\nu)}{2}=\frac{1}{2}\left[1-e^{-\nu}\sum_{j=0}^{M-1}\frac{\nu^j}{j!}\right], \tag{35}$$

which is independent of the energy of the pulses $\alpha^2$.

**Hybrid receiver.** When considering the hybrid receiver, the presence of dark counts affects also homodyne-like detection. Indeed, the probability of obtaining the photocurrent difference $\Delta=-M,\ldots,M$ reads

$$\mathcal{S}_\nu\left(\Delta;\alpha_{0/1}^{(r)}\right)=\sum_{n=0}^{M}\sum_{m=0}^{M}\delta_{n-m,\Delta}\,p^{(M)}\left(n;\mu_c\left(\alpha_{0/1}^{(r)}\right)+\nu\right)p^{(M)}\times\left(m;\mu_d\left(\alpha_{0/1}^{(r)}\right)+\nu\right). \tag{36}$$

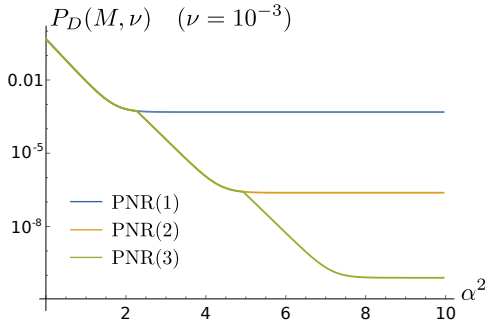


**Fig. 5.** Logarithmic plot of the error probability for the displacement-PNR($M$) receiver as a function of $\alpha^2$ for several values of $M$. The dark count rate is set to $\nu=10^{-3}$.

**Table 2. Decision Rule for Hybrid Receiver in Presence of Dark Counts**

| Outcomes | Decision |
|---|---|
| $\Delta \geq 0$ $n < n_{\rm th}(\nu)$ | 0 |
| $\Delta < 0$ $n \geq n_{\rm th}(\nu)$ | 0 |
| $\Delta < 0$ $n < n_{\rm th}(\nu)$ | 1 |
| $\Delta \geq 0$ $n \geq n_{\rm th}(\nu)$ | 1 |

Given all the previous considerations, the decision rule for the hybrid receiver in the presence of dark counts should be modified into that of Table 2. The error probability then reads

$$
\begin{aligned}
P_{\rm hyb}^{(M)}(\tau;\nu) &= q_0\,[p(\Delta<0, n<n_{\rm th}(\nu)|0)+p(\Delta\geq 0, n\geq n_{\rm th}(\nu)|0)] \\
&\quad + q_1\,[p(\Delta<0, n\geq n_{\rm th}(\nu)|1)+p(\Delta\geq 0, n< n_{\rm th}(\nu)|1)] \\
&= \frac{1}{2}\sum_{n=0}^{n_{\rm th}(\nu)-1} p^{(M)}(n;4\tau\alpha^2+\nu)\left[\sum_{\Delta=-M}^{-1}\mathcal{S}_\nu(\Delta;\alpha_0^{(r)})+\sum_{\Delta=0}^{M}\mathcal{S}_\nu(\Delta;\alpha_1^{(r)})\right] \\
&\quad + \frac{1}{2}\sum_{n=n_{\rm th}(\nu)}^{M} p^{(M)}(n;\nu)\left[\sum_{\Delta=-M}^{-1}\mathcal{S}_\nu(\Delta;\alpha_1^{(r)})+\sum_{\Delta=0}^{M}\mathcal{S}_\nu(\Delta;\alpha_0^{(r)})\right].
\end{aligned}
\tag{37}
$$

The optimized error probability $P_{\rm hyb}^{(M)}(\tau_{\rm opt}(M,\nu);\nu)$ is depicted in the top panel of Fig. 6, whereas the optimized transmissivity $\tau_{\rm opt}(M,\nu)$ is depicted in its bottom panel. For better visualization of the advantages brought by the hybrid receiver with respect to the D-PNRM, in the inset of Fig. 6 (top panel),

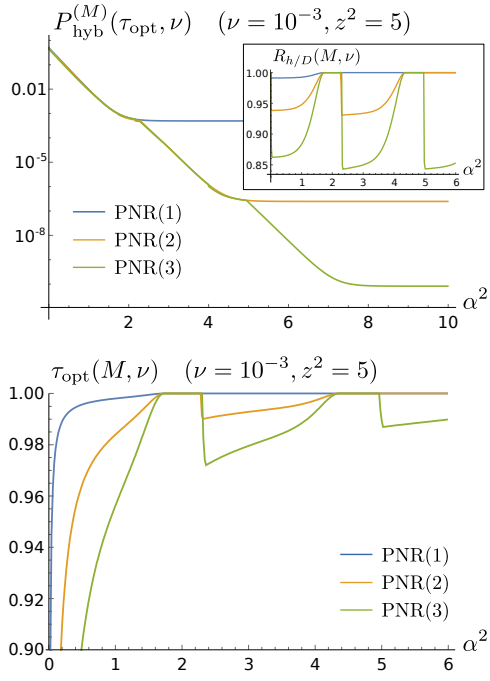


**Fig. 6.** (Top) Logarithmic plot of the error probability for the hybrid receiver employing PNR($M$) detectors as a function of $\alpha^2$ for several values of $M$. In the inset, plot of the ratio $R_{h/D}(M,\nu)$ as a function of $\alpha^2$. (Bottom) Plot of the optimized $\tau_{\rm opt}(M,\nu)$ as a function of $\alpha^2$ for several $M$. Here the dark count rate is set to the value $\nu=10^{-3}$, and the LO for the homodyne-like detector is $z^2=5$.

we plot also the ratio

$$
R_{h/D}(M,\nu)=\frac{P_{\rm hyb}^{(M)}(\tau_{\rm opt}(M,\nu);\nu)}{P_D(M,\nu)}. \tag{38}
$$

The behavior is different from that of Section 4: first, the value of $\tau_{\rm opt}(M,\nu)$ increases with $\alpha^2$ until reaching exactly the value 1, i.e., performing as a D-PNRM. Accordingly, the ratio $R_{h/D}(M,\nu)$ does not saturate but shows a plateau, after which increasing towards 1. For larger energies, according to the resolution $M$, there appear $M-1$ "sawteeth," that is, other $M-1$ regions in which $\tau_{\rm opt}(M,\nu)$ [and $R_{h/D}(M,\nu)$ together with it] decreases to a value smaller than 1 and increases further to again reach 1. Finally, given the results of the previous subsection, we note that if a quantum efficiency $\eta<1$ were also present, its only effect would be the modification of the plateau value of $R_{h/D}(M,\nu)$, preserving the same qualitative behavior.

### D. Visibility $\xi$

Finally, we address the effect of the interference visibility $\xi\leq 1$ of the displacement operations employed in the realization of the receiver. This effect is a consequence of the mode mismatch at the beam splitter, which implements practically a displacement. The value $\xi<1$ quantifies the overlap between the spatial areas of the signal and the auxiliary field mixed at the beam splitter. As discussed in [11,25], a reduction in visibility affects crucially the performances of quantum receivers.

Generally speaking, we consider a coherent state $|\zeta\rangle$ that we want to displace by a quantity $\beta$ into the state $|\zeta+\beta\rangle$. For the sake of simplicity, we assume $\zeta,\beta\in\mathbb{R}$. Then, we can describe the effect induced by imperfect mode matching by stating that the outcome $n$ of the subsequent PNR measurement follows a Poisson distribution with rate $N=\zeta^2+\beta^2+2\xi\zeta\beta\neq(\zeta+\beta)^2$. As in the previous subsection, we first analyze the cases of the D-PNRM receiver and then address the hybrid receiver. As before, we fix $\eta=1$.

**D-PNRM receiver.** In the presence of visibility reduction, the approach is quite similar to Section 5.C. If $|\alpha_0\rangle$ is sent, the probability of detecting outcome $n$ is $p^{(M)}(n;2\alpha^2(1-\xi))$, whereas for $|\alpha_1\rangle$, the probability is $p^{(M)}(n;2\alpha^2(1+\xi))$. By following the MAP criterion, the error probability then reads

$$P_D(M,\xi) = 1 - \frac{1}{2}\sum_{n=0}^{M} \max\left[p^{(M)}(n; g_-),\, p^{(M)}(n; g_+)\right], \tag{39}$$

where

$$g_\pm = 2\alpha^2(1 \pm \xi), \tag{40}$$

associated with the threshold outcome $n_{\rm th}(\xi)$:

$$n_{\rm th}(\xi) = \min\left[\left\lceil \frac{4\xi\alpha^2}{\ln(1+\xi) - \ln(1-\xi)} \right\rceil, M\right]. \tag{41}$$

We recall that the case of PNR(1) is equivalent to the on–off Kennedy receiver. The consequences of a $<1$ visibility on error probabilities is shown in Fig. 7. For dark counts, visibility reduction makes the error probability nonmonotonic, and in particular increasing for large $\alpha^2$. As before, this is a consequence of the finite resolution $M$. In the regime of large $\alpha^2$, the threshold outcome becomes $n_{\rm th}(\xi) = M$; thus, the error probability is due to outcomes $M$ induced by the state $|\alpha_0\rangle$, which is not perfectly "nulled" due to the imperfect displacement operation. Therefore, we have

$$P_D(M,\xi) \approx \frac{p^{(M)}(M; g_-)}{2} = \frac{1}{2}\left[1 - e^{-2\alpha^2(1-\xi)} \sum_{j=0}^{M-1} \frac{(2\alpha^2(1-\xi))^j}{j!}\right], \tag{42}$$

which is an increasing function of $\alpha^2$.

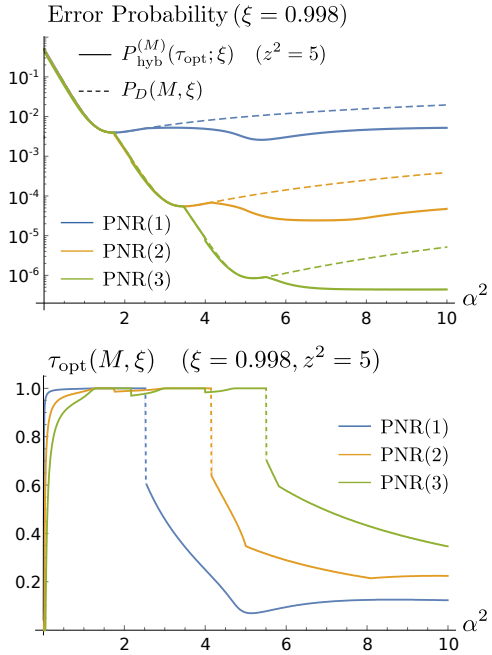


**Fig. 7.** (Top) Logarithmic plot of the error probability for the hybrid receiver employing PNR($M$) detectors and the displacement-PNR($M$) receiver as a function of $\alpha^2$ for several values of $M$. (Bottom) Plot of the optimized $\tau_{\rm opt}(M,\xi)$ as a function of $\alpha^2$ for several $M$. Here the visibility is set to the value $\xi = 0.998$, and the LO for the homodyne-like detector is $z^2 = 5$.

**Table 3. Decision Rule for Hybrid Receiver in Presence of Visibility Reduction**

| Outcomes | Decision |
|---|---|
| $\Delta \geq 0$ $n < n_{\rm th}(\xi)$ | 0 |
| $\Delta < 0$ $n \geq n_{\rm th}(\xi)$ | 0 |
| $\Delta < 0$ $n < n_{\rm th}(\xi)$ | 1 |
| $\Delta \geq 0$ $n \geq n_{\rm th}(\xi)$ | 1 |

**Hybrid receiver.** For the hybrid receiver, we should also include visibility reduction in the balanced beam splitter inside the homodyne-like detector. As a consequence, the probability of measuring the photocurrent $\Delta = -M, \ldots, M$ is changed into

$$\mathcal{S}_\xi\left(\Delta; \alpha^{(r)}_{0/1}\right) = \sum_{n=0}^{M}\sum_{m=0}^{M} \delta_{n-m,\Delta}\, p^{(M)}\left(n; \tilde{\mu}_c\left(\alpha^{(r)}_{0/1}; \xi\right)\right) p^{(M)} \times \left(m; \tilde{\mu}_d\left(\alpha^{(r)}_{0/1}; \xi\right)\right), \tag{43}$$

where

$$\tilde{\mu}_c(\alpha^{(r)}_{0/1}; \xi) = \frac{\left(\alpha^{(r)}_{0/1}\right)^2 + z^2 + 2\xi\, z\alpha^{(r)}_{0/1}}{2}, \tag{44a}$$

$$\tilde{\mu}_d(\alpha^{(r)}_{0/1}; \xi) = \frac{\left(\alpha^{(r)}_{0/1}\right)^2 + z^2 - 2\xi\, z\alpha^{(r)}_{0/1}}{2}, \tag{44b}$$

where $p^{(M)}(n;\, N)$ is the same as in Eq. (25).

The decision rule for the hybrid receiver, displayed in Table 3, is identical to the case of dark counts. The error probability then reads

$$\begin{aligned} P^{(M)}_{\rm hyb}(\tau;\xi) &= q_0\left[p(\Delta<0,\, n<n_{\rm th}(\xi)|0) + p(\Delta\geq 0,\, n\geq n_{\rm th}(\xi)|0)\right] \\ &\quad + q_1\left[p(\Delta<0,\, n\geq n_{\rm th}(\xi)|1) + p(\Delta\geq 0,\, n<n_{\rm th}(\xi)|1)\right] \\ &= \frac{1}{2}\sum_{n=0}^{n_{\rm th}(\xi)-1} p^{(M)}(n;\tau g_+) \times\left[\sum_{\Delta=-M}^{-1}\mathcal{S}_\xi(\Delta;\alpha_0^{(r)}) + \sum_{\Delta=0}^{M}\mathcal{S}_\xi(\Delta;\alpha_1^{(r)})\right] \\ &\quad + \frac{1}{2}\sum_{n=n_{\rm th}(\xi)}^{M} p^{(M)}(n;\tau g_-) \times\left[\sum_{\Delta=-M}^{-1}\mathcal{S}_\xi(\Delta;\alpha_1^{(r)}) + \sum_{\Delta=0}^{M}\mathcal{S}_\xi(\Delta;\alpha_0^{(r)})\right]. \end{aligned} \tag{45}$$

Figure 7 shows the optimized $\tau_{\rm opt}(M,\xi)$ and the optimized probability $P^{(M)}_{\rm hyb}(\tau_{\rm opt}(M,\xi);\xi)$. If $\alpha^2$ is small, we have a

behavior similar to the dark count case, but for large $\alpha^2$, the transmissivity changes discontinuously, and the resulting $P_{\rm hyb}^{(M)}(\tau_{\rm opt}(M,\xi);\xi)$ always stays below $P_D(M,\xi)$. This shows that by choosing appropriately the energy of the signals undergoing homodyne-like and D-PNR measurements, it is possible to regain part of the information lost to the finite resolution of the detectors. As a result, the interplay between the two schemes allows to mitigate the negative effects introduced by visibility reduction.

## 6. CONCLUSION

In this paper, we have advanced the proposal of a new hybrid receiver for binary coherent discrimination, based on the combination of homodyne-like and Kennedy setups. The incoming signal is split at a beam splitter of variable transmissivity $\tau$, and the reflected beam undergoes homodyne-like detection, whose outcome determines a conditioned displacement operation on the transmitted beam, followed by on–off measurement. We have shown that the possibility of adjusting the value of $\tau$ for every value of the energy (for example, by exploiting a polarizing beam splitter) makes such receiver near-optimum and capable of beating both the SQL, i.e., the homodyne error probability in Eq. (11), and the Kennedy limit.

Moreover, we have shown that the receiver proves to be robust against the presence of inefficiencies of the experimental setup implementing the receiver, making it a valuable option for realistic experimental implementations of binary receivers. In particular, we have shown that in the presence of a finite resolution $M$ of the PNR detector, an appropriate choice of transmissivity $\tau$ makes the hybrid receiver beat the performances of the sole D-PNR($M$) receiver. Indeed, the possibility of splitting the energy of the coherent seed into two branches allows to regain part of the information lost because of the finite resolution of the detector.

Further advantages in the regime of small energies may be obtained by following the philosophy of the improved Kennedy receiver [5], that is, by optimizing also the amplitude of the displacement operation conditioned on the homodyne-like outcome $\Delta$. By considering an optimized displacement $D(\mp\beta_{\rm opt})$, we expect to maintain the quasi-optimality of the receiver and also to reduce the error probabilities for energies $\alpha^2 < 1$.

The homodyne-like scheme used together with other kinds of receivers can lead to enhancing their performances. For instance, promising results can be obtained combining it with displacement receivers with feed-forward operations [9,10], thus fostering further research in this direction.

## APPENDIX A: MAXIMUM A POSTERIORI PROBABILITY CRITERION

We consider a generic displacement photon counting discrimination scheme to discriminate between coherent states $|-\alpha\rangle$ and $|\alpha\rangle$ ($\alpha\in\mathbb{R}_+$) generated with equal *a priori* probabilities $p(\mp\alpha)=1/2$. We apply a fixed displacement of $\beta$ onto the incoming signal, mapping the states into

$$|\pm\alpha\rangle \to |\pm\alpha+\beta\rangle. \tag{A1}$$

Then we perform a PNR measurement on the displaced state. The MAP criterion states that, given the outcome $n$, we infer the state with the highest *a posteriori* probability:

$$p(\mp\alpha|n)=\frac{p(n|\pm\alpha)\;p(\mp\alpha)}{p(n)}, \tag{A2}$$

where

$$p(n|\pm\alpha)=e^{-|\pm\alpha+\beta|^2}\frac{|\pm\alpha+\beta|^{2n}}{n!} \tag{A3}$$

is the probability of getting $n$ photons given $\pm\alpha$, and

$$p(n)=p(\alpha)p(n|\alpha)+p(-\alpha)p(n|-\alpha)=\frac{p(n|\alpha)+p(n|-\alpha)}{2}$$

is the global probability of detecting $n$ photons. For example, we infer $|-\alpha\rangle$ if $p(-\alpha|n)>p(\alpha|n)$, which is equivalent to the condition $p(n|-\alpha)>p(n|\alpha)$ since we have $p(\mp\alpha)=1/2$.

The correct decision probability is then equal to

$$P_c=p(-\alpha)\sum_{n=0}^{\infty}p(n|-\alpha)\chi_{-\alpha}+p(\alpha)\sum_{n=0}^{\infty}p(n|\alpha)\chi_{\alpha} \tag{A4}$$

$$=\frac{1}{2}\sum_{n=0}^{\infty}\max[p(n|-\alpha),\,p(n|\alpha)], \tag{A5}$$

where $\chi_{-\alpha}=1$ if $p(n|-\alpha)>p(n|\alpha)$ and zero otherwise, and $\chi_{\alpha}=1$ if $p(n|\alpha)>p(n|-\alpha)$ and zero otherwise. The error probability is obtained immediately as $P_{\rm err}=1-P_c$.

The decision rule $p(n|-\alpha)\lesseqgtr p(n|\alpha)$ is equivalent to the definition of a threshold outcome $n_{\rm th}$ such that all measurement outcomes $n\geq n_{\rm th}$ are assigned to state $\alpha$, and all $n<n_{\rm th}$ are assigned to state $-\alpha$. The threshold number is obtained by equating $p(n_{\rm th}|-\alpha)=p(n_{\rm th}|\alpha)$ and reads

$$n_{\rm th}=\left\lceil\frac{|\alpha+\beta|^2-|\alpha-\beta|^2}{\ln(|\alpha+\beta|^2)-\ln(|\alpha-\beta|^2)}\right\rceil, \tag{A6}$$

where $\lceil x\rceil$ is the ceiling function, returning the smallest integer greater than $x$.

Finally, we note that for the standard Kennedy receiver, the displacement amplitude is $\beta=\alpha$, such that $p(n|-\alpha)=\delta_{n,0}$, and therefore, the correct probability of Eq. (A5) reduces to $P_c=1-\exp(-4\alpha^2)/2$.

**Funding.** Università degli Studi di Milano (RV-PSR-SOE-2020-SOLIV "S–O PhoQuLis"); Ministero degli Affari Esteri e della Cooperazione Internazionale (PGR06314 "ENYGMA").

**Disclosures.** The authors declare no conflicts of interest.

**Data availability.** Data underlying the results presented in this paper are not publicly available at this time but may be obtained from the authors upon reasonable request.

## REFERENCES

1. G. Cariolaro, *Quantum Communications* (Springer, 2015).
2. C. W. Helstrom, *Quantum Detection and Estimation Theory* (Elsevier/Academic, 1976).
3. J. A. Bergou, "Discrimination of quantum states," J. Mod. Opt. **57**, 160–180 (2010).

4. R. S. Kennedy, "A near-optimum receiver for the binary coherent state quantum channel," Quart. Prog. Rep. **108**, 219–225 (1973).
5. M. Takeoka and M. Sasaki, "Discrimination of the binary coherent signal: Gaussian-operation limit and simple non-Gaussian near-optimal receivers," Phys. Rev. A **78**, 022320 (2008).
6. M. Sasaki and O. Hirota, "Optimum decision scheme with a unitary control process for binary quantum-state signals," Phys. Rev. A **54**, 2728–2736 (1996).
7. S. J. Dolinar, "An optimum receiver for the binary coherent state quantum channel," Quart. Prog. Rep. **11**, 115–120 (1973).
8. M. Takeoka, M. Sasaki, and N. Lütkenhaus, "Binary projective measurement via linear optics and photon counting," Phys. Rev. Lett. **97**, 040502 (2006).
9. A. Assalini, N. D. Pozza, and G. Pierobon, "Revisiting the Dolinar receiver through multiple-copy state discrimination theory," Phys. Rev. A **84**, 022342 (2011).
10. D. Sych and G. Leuchs, "Practical receiver for optimal discrimination of binary coherent signals," Phys. Rev. Lett. **117**, 200501 (2016).
11. M. T. DiMario and F. E. Becerra, "Robust measurement for the discrimination of binary coherent states," Phys. Rev. Lett. **121**, 023603 (2018).
12. A. Allevi, M. Bina, S. Olivares, and M. Bondani, "Homodyne-like detection scheme based on photon-number-resolving detectors," Int. J. Quantum Inf. **15**, 1740016 (2017).
13. M. Bina, A. Allevi, M. Bondani, and S. Olivares, "Homodyne-like detection for coherent state-discrimination in the presence of phase noise," Opt. Express **25**, 10685–10692 (2017).
14. S. Olivares, A. Allevi, G. Caiazzo, M. G. A. Paris, and M. Bondani, "Quantum tomography of light states by photon-number-resolving detectors," New J. Phys. **21**, 103045 (2019).
15. G. S. Thekkadath, D. S. Phillips, J. F. F. Bulmer, W. R. Clements, A. Eckstein, B. A. Bell, J. Lugani, T. A. W. Wolterink, A. Lita, S. W. Nam, T. Gerrits, C. G. Wade, and I. A. Walmsley, "Tuning between photon-number and quadrature measurements with weak-field homodyne detection," Phys. Rev. A **101**, 031801 (2020).
16. R. Nehra, M. Eaton, C. González-Arciniegas, M. S. Kim, T. Gerrits, A. Lita, S. W. Nam, and O. Pfister, "Generalized overlap quantum state tomography," Phys. Rev. Res. **2**, 042002 (2020).
17. S. Olivares, "Introduction to generation, manipulation and characterization of optical quantum states," Phys. Lett. A **418**, 127720 (2021).
18. S. Olivares, A. Allevi, and M. Bondani, "On the role of the local oscillator intensity in optical homodyne-like tomography," Phys. Lett. A **384**, 126354 (2020).
19. G. Humer, M. Peev, C. Schaeff, S. Ramelow, M. Stipčević, and R. Ursin, "A simple and robust method for estimating afterpulsing in single photon detectors," J. Lightwave Technol. **33**, 3098–3107 (2015).
20. S. Izumi, M. Takeoka, M. Fujiwara, N. D. Pozza, A. Assalini, K. Ema, and M. Sasaki, "Displacement receiver for phase-shift-keyed coherent states," Phys. Rev. A **86**, 042328 (2012).
21. S. Izumi, J. S. Neergaard-Nielsen, and U. L. Andersen, "Adaptive generalized measurement for unambiguous state discrimination of quaternary phase-shift-keying coherent states," PRX Quantum **2**, 020305 (2021).
22. M. T. DiMario, E. Carrasco, R. A. Jackson, and F. E. Becerra, "Implementation of a single-shot receiver for quaternary phase-shift keyed coherent states," J. Opt. Soc. Am. B **35**, 568–574 (2018).
23. G. S. Thekkadath, S. Sempere-Llagostera, B. A. Bell, R. B. Patel, M. S. Kim, and I. A. Walmsley, "Single-shot discrimination of coherent states beyond the standard quantum limit," Opt. Lett. **46**, 2565–2568 (2021).
24. J. S. Sidhu, S. Izumi, J. S. Neergaard-Nielsen, C. Lupo, and U. L. Andersen, "Quantum receiver for phase-shift keying at the single-photon level," PRX Quantum **2**, 010332 (2021).
25. F. E. Becerra, J. Fan, and A. Migdall, "Photon number resolution enables quantum receiver for realistic coherent optical communications," Nat. Photonics **9**, 48–53 (2015).